



# GROWTH on S190425z: Searching Thousands of Square Degrees to Identify an Optical or Infrared Counterpart to a Binary Neutron Star Merger with the Zwicky Transient Facility and Palomar Gattini-IR

Michael W. Coughlin<sup>1</sup>, Tomás Ahumada<sup>2</sup>, Shreya Anand<sup>1</sup>, Kishalay De<sup>1</sup>, Matthew J. Hankins<sup>1</sup>, Mansi M. Kasliwal<sup>1</sup>, Leo P. Singer<sup>3,4</sup>, Eric C. Bellm<sup>5</sup>, Igor Andreoni<sup>1</sup>, S. Bradley Cenko<sup>3,4</sup>, Jeff Cooke<sup>6,7</sup>, Christopher M. Copperwheat<sup>8</sup>, Alison M. Dugas<sup>1</sup>, Jacob E. Jencson<sup>1</sup>, Daniel A. Perley<sup>8</sup>, Po-Chieh Yu<sup>9</sup>, Varun Bhalerao<sup>10</sup>, Harsh Kumar<sup>10</sup>, Joshua S. Bloom<sup>11,12</sup>, G. C. Anupama<sup>13</sup>, Michael C. B. Ashley<sup>14</sup>, Ashot Bagdasaryan<sup>1</sup>, Rahul Biswas<sup>15</sup>, David A. H. Buckley<sup>16,17</sup>, Kevin B. Burdge<sup>1</sup>, David O. Cook<sup>18</sup>, John Cromer<sup>19</sup>, Virginia Cunningham<sup>2</sup>, Antonino D’Ai<sup>20</sup>, Richard G. Dekany<sup>19</sup>, Alexandre Delacroix<sup>19</sup>, Simone Dichiara<sup>2,3</sup>, Dmitry A. Duev<sup>1</sup>, Anirban Dutta<sup>13</sup>, Michael Feeney<sup>19</sup>, Sara Frederick<sup>2</sup>, Pradip Gatkine<sup>2</sup>, Shaon Ghosh<sup>21</sup>, Daniel A. Goldstein<sup>1</sup>, V. Zach Golkhou<sup>5,22,40</sup>, Ariel Goobar<sup>15</sup>, Matthew J. Graham<sup>1</sup>, Hidekazu Hanayama<sup>23</sup>, Takashi Horiuchi<sup>23</sup>, Tiara Hung<sup>24</sup>, Saurabh W. Jha<sup>25,26</sup>, Albert K. H. Kong<sup>27</sup>, Matteo Giomì<sup>28</sup>, David L. Kaplan<sup>21</sup>, V. R. Karambelkar<sup>10</sup>, Marek Kowalski<sup>29,30</sup>, Shrinivas R. Kulkarni<sup>1</sup>, Thomas Kupfer<sup>31</sup>, Frank J. Masci<sup>18</sup>, Paolo Mazzali<sup>8</sup>, Anna M. Moore<sup>32</sup>, Moses Mogotsi<sup>16,17</sup>, James D. Neill<sup>1</sup>, Chow-Choong Ngeow<sup>9</sup>, Jorge Martínez-Palomera<sup>33</sup>, Valentina La Parola<sup>20</sup>, M. Pavana<sup>13</sup>, Eran O. Ofek<sup>34</sup>, Atharva Sunil Patil<sup>9</sup>, Reed Riddle<sup>19</sup>, Mickael Rigault<sup>35</sup>, Ben Rusholme<sup>18</sup>, Eugene Serabyn<sup>36</sup>, David L. Shupe<sup>18</sup>, Yashvi Sharma<sup>10</sup>, Avinash Singh<sup>13</sup>, Jesper Sollerman<sup>37</sup>, Jamie Soon<sup>32</sup>, Kai Staats<sup>38</sup>, Kirsty Taggart<sup>8</sup>, Hanjie Tan<sup>9</sup>, Tony Travoignon<sup>32</sup>, Eleonora Troja<sup>2,3</sup>, Gaurav Waratkar<sup>10</sup>, and Yoichi Yatsu<sup>39</sup>

<sup>1</sup> Division of Physics, Mathematics, and Astronomy, California Institute of Technology, Pasadena, CA 91125, USA

<sup>2</sup> Department of Astronomy, University of Maryland, College Park, MD 20742, USA

<sup>3</sup> Astrophysics Science Division, NASA Goddard Space Flight Center, MC 661, Greenbelt, MD 20771, USA

<sup>4</sup> Joint Space-Science Institute, University of Maryland, College Park, MD 20742, USA

<sup>5</sup> DIRAC Institute, Department of Astronomy, University of Washington, 3910 15th Avenue NE, Seattle, WA 98195, USA

<sup>6</sup> Australian Research Council Centre of Excellence for Gravitational Wave Discovery (OzGrav), Swinburne University of Technology, Hawthorn, VIC, 3122, Australia

<sup>7</sup> Centre for Astrophysics and Supercomputing, Swinburne University of Technology, Hawthorn, VIC, 3122, Australia

<sup>8</sup> Astrophysics Research Institute, Liverpool John Moores University, IC2, Liverpool Science Park, 146 Brownlow Hill, Liverpool L3 5RF, UK

<sup>9</sup> Graduate Institute of Astronomy, National Central University, 32001, Taiwan

<sup>10</sup> Indian Institute of Technology Bombay, Powai, Mumbai 400076, India

<sup>11</sup> Department of Astronomy, University of California, Berkeley, CA 94720-3411, USA

<sup>12</sup> Physics, Lawrence Berkeley National Laboratory, 1 Cyclotron Road, MS 50B-4206, Berkeley, CA 94720, USA

<sup>13</sup> Indian Institute of Astrophysics, II Block Koramangala, Bengaluru 560034, India

<sup>14</sup> School of Physics, University of New South Wales, Sydney NSW 2052, Australia

<sup>15</sup> The Oskar Klein Centre, Department of Physics, Stockholm University, AlbaNova, SE-106 91 Stockholm, Sweden

<sup>16</sup> South African Astronomical Observatory, P.O. Box 9, Observatory 7935, Cape Town, South Africa

<sup>17</sup> Southern African Large Telescope Foundation, P.O. Box 9, Observatory 7935, Cape Town, South Africa

<sup>18</sup> IPAC, California Institute of Technology, 1200 E. California Blvd, Pasadena, CA 91125, USA

<sup>19</sup> Caltech Optical Observatories, California Institute of Technology, Pasadena, CA 91125, USA

<sup>20</sup> INAF/IASF-Palermo, via Ugo La Malfa 153, I-90146, Palermo, Italy

<sup>21</sup> Center for Gravitation, Cosmology and Astrophysics, Department of Physics, University of Wisconsin–Milwaukee, P.O. Box 413, Milwaukee, WI 53201, USA

<sup>22</sup> The eScience Institute, University of Washington, Seattle, WA 98195, USA

<sup>23</sup> Ishigakijima Astronomical Observatory, National Astronomical Observatory of Japan, 1024-1 Arakawa, Ishigaki, Okinawa 907-0024, Japan

<sup>24</sup> Department of Astronomy and Astrophysics, University of California, Santa Cruz, CA 95064, USA

<sup>25</sup> Department of Physics and Astronomy, Rutgers, the State University of New Jersey, 136 Frelinghuysen Road, Piscataway, NJ 08854, USA

<sup>26</sup> Center for Computational Astrophysics, Flatiron Institute, 162 5th Avenue, New York, NY 10010, USA

<sup>27</sup> Institute of Astronomy, National Tsing Hua University, Hsinchu 30013, Taiwan

<sup>28</sup> Humboldt Universität zu Berlin, Newtonstraße 15, D-12489 Berlin, Germany

<sup>29</sup> Institute of Physics, Humboldt-Universität zu Berlin, Newtonstr. 15, D-124 89 Berlin, Germany

<sup>30</sup> Deutsches Elektronensynchrotron, Platanenallee 6, D-15738, Zeuthen, Germany

<sup>31</sup> Kavli Institute for Theoretical Physics, University of California, Santa Barbara, CA 93106, USA

<sup>32</sup> Research School of Astronomy and Astrophysics, Australian National University, Canberra, ACT 2611, Australia

<sup>33</sup> Department of Astronomy, University of California, Berkeley, CA 94720-3411, USA

<sup>34</sup> Department of Particle Physics & Astrophysics, Weizmann Institute of Science, Rehovot 76100, Israel

<sup>35</sup> Université Clermont Auvergne, CNRS/IN2P3, Laboratoire de Physique de Clermont, F-63000 Clermont-Ferrand, France

<sup>36</sup> Jet Propulsion Laboratory, California Institute of Technology, Pasadena, CA 91109, USA

<sup>37</sup> The Oskar Klein Centre & Department of Astronomy, Stockholm University, AlbaNova, SE-106 91 Stockholm, Sweden

<sup>38</sup> Center for Interdisciplinary Exploration and Research in Astrophysics and Department of Physics and Astronomy, Northwestern University, 2145 Sheridan Road, Evanston, IL 60208, USA

<sup>39</sup> Department of Physics, Tokyo Institute of Technology, 2-12-1, Ookayama, Meguro, Tokyo 152-8551, Japan

Received 2019 July 29; revised 2019 September 24; accepted 2019 October 4; published 2019 October 30

<sup>40</sup> Moore-Sloan, WRF, and DIRAC Fellow.

## Abstract

The third observing run by LVC has brought the discovery of many compact binary coalescences. Following the detection of the first binary neutron star merger in this run (LIGO/Virgo S190425z), we performed a dedicated follow-up campaign with the Zwicky Transient Facility (ZTF) and Palomar Gattini-IR telescopes. The initial skymap of this single-detector gravitational wave (GW) trigger spanned most of the sky observable from Palomar Observatory. Covering 8000 deg<sup>2</sup> of the initial skymap over the next two nights, corresponding to 46% integrated probability, ZTF system achieved a depth of  $\approx 21 m_{AB}$  in  $g$ - and  $r$ -bands. Palomar Gattini-IR covered 2200 square degrees in  $J$ -band to a depth of 15.5 mag, including 32% integrated probability based on the initial skymap. The revised skymap issued the following day reduced these numbers to 21% for the ZTF and 19% for Palomar Gattini-IR. We narrowed 338,646 ZTF transient “alerts” over the first two nights of observations to 15 candidate counterparts. Two candidates, ZTF19aarykbb and ZTF19aarzaod, were particularly compelling given that their location, distance, and age were consistent with the GW event, and their early optical light curves were photometrically consistent with that of kilonovae. These two candidates were spectroscopically classified as young core-collapse supernovae. The remaining candidates were ruled out as supernovae. Palomar Gattini-IR did not identify any viable candidates with multiple detections only after merger time. We demonstrate that even with single-detector GW events localized to thousands of square degrees, systematic kilonova discovery is feasible.

*Unified Astronomy Thesaurus concepts:* [Gravitational wave astronomy \(675\)](#); [Transient detection \(1957\)](#); [Optical telescopes \(1174\)](#)

## 1. Introduction

The third observing run (O3) by the network of gravitational-wave (GW) detectors with Advanced LIGO (Aasi et al. 2015) and Advanced Virgo (Acernese et al. 2015) began in 2019 April. This detector network has already observed over a score binary black holes thus far (LIGO Scientific Collaboration & Virgo Collaboration 2019a, 2019b, 2019c, 2019d, 2019e, 2019f). The current discovery rate builds on the success of the first few observing runs, which yielded 10 binary black hole detections (Abbott et al. 2019).

In addition, the coincident discovery of the binary neutron star (BNS) merger GW170817 (Abbott et al. 2017a), a short gamma-ray burst (SGRB) GRB170817A (Abbott et al. 2017b; Goldstein et al. 2017; Savchenko et al. 2017), with an afterglow (Alexander et al. 2017; Haggard et al. 2017; Hallinan et al. 2017; Margutti et al. 2017; Troja et al. 2017) and “kilonova” (KN) counterpart, AT2017gfo (Chornock et al. 2017; Coulter et al. 2017; Cowperthwaite et al. 2017; Drout et al. 2017; Evans et al. 2017; Kasliwal et al. 2017; Kilpatrick et al. 2017; Lipunov et al. 2017; McCully et al. 2017; Nicholl et al. 2017; Pian et al. 2017; Shappee et al. 2017; Smartt et al. 2017; Utsumi et al. 2017), initiated a new era of multi-messenger astronomy. Among many other science cases, measurements of the equation of state of neutron stars (Bauswein et al. 2013, 2017; Abbott et al. 2017a; Radice et al. 2018; Coughlin et al. 2019f), the formation of heavy elements (Just et al. 2015; Wu et al. 2016; Abbott et al. 2017c; Roberts et al. 2017; Rosswog et al. 2017; Kasliwal et al. 2019a), and the expansion rate of the universe (Abbott et al. 2017d; Hotokezaka et al. 2018; Coughlin et al. 2019e) are all important results of the first BNS detection.

Following the success of GW170817, the Zwicky Transient Facility (ZTF; Bellm et al. 2018; Masci et al. 2018; Dekany et al. 2019; Graham et al. 2019) on the Palomar 48 inch telescope, and Palomar Gattini-IR, a new wide-field near-infrared survey telescope at Palomar observatory, have been observing both SGRBs from the *Fermi* Gamma-ray Burst Monitor (Ahumada et al. 2018; Coughlin et al. 2018b, 2018c, 2018d, 2018e, 2019a; Cenko et al. 2018) and GW events from LIGO. In addition to finding the “afterglow” associated with a

highly relativistic jet powered by an SGRB (Wijers et al. 1997; Mészáros & Rees 1998; Ascenzi et al. 2019), our goal has been to identify a KN, the ultraviolet/optical/near-infrared (near-IR) emission generated by the radioactive decay of  $r$ -process elements (Lattimer & Schramm 1974; Li & Paczynski 1998; Metzger et al. 2010; Roberts et al. 2011; Rosswog 2015; Kasen et al. 2017). The ZTF and Palomar Gattini-IR surveys are our discovery engines, and the Global Relay of Observatories Watching Transients Happen (GROWTH) network<sup>41</sup> is our follow-up network. GROWTH uses a variety of facilities worldwide across various wavelengths to perform rapid follow-up and classification of objects.

There are many survey systems participating in the searches for GW counterparts. Among many others, the Dark Energy Camera (DECam; Flaugher et al. 2015), the Gravitational-wave Optical Transient Observer (GOTO; O’Brien 2018), the Panoramic Survey Telescope and Rapid Response System (Pan-STARRS; Kaiser et al. 2010; Chambers et al. 2016), the All-Sky Automated Survey for Supernovae (ASASSN; Shappee et al. 2014) and Asteroid Terrestrial-impact Last Alert System (ATLAS; Tonry et al. 2018) all have performed observations of events during the third observing run. ZTF provides a competitive addition to these systems, given its depth ( $m_{AB} \sim 20.6$  in 30 s), wide field of view (FOV  $\approx 47$  deg<sup>2</sup> per exposure), and average cadence of  $\sim 3$  days over the entire accessible sky. In particular, the cadence is important for establishing candidate history when performing target of opportunity (ToO) observations. The SGRB program, that has covered localization regions spanning thousands of square degrees (Coughlin et al. 2019a), demonstrated that ZTF is capable of detecting GW170817-like sources out to the Advanced LIGO/Virgo detection horizon at about ( $\sim 200$  Mpc; Abbott et al. 2018). In addition, Palomar Gattini-IR (K. De et al. 2019, in preparation; Moore & Kasliwal 2019) is covering the entire visible northern sky every two nights to a  $J$ -band depth of  $\approx 15.5$ –16 AB mag. With its 25 deg<sup>2</sup> FOV and near-IR sensitivity, Palomar Gattini-IR provides a complementary system for objects that are expected to be as red as KNe

<sup>41</sup> <http://growth.caltech.edu/>

**Table 1**  
Telescope Specifications, Including Name, FOV, Pixel Scale, Telescope Aperture, and Available Filters

Name	FOV	Pixel Scale	Aperture	Filters
ZTF	47 deg <sup>2</sup>	1''0	48 in	<i>g, r, i</i>
Palomar Gattini-IR	25 deg <sup>2</sup>	8''7	30 cm	<i>J</i>
GROWTH-India	0.5 deg <sup>2</sup>	0''67	70 cm	<i>u, g, r, i, z</i>
LOT	13'2 × 13'2	0''39	1 m	<i>g, r, i</i>
KPED	4'4 × 4'4	0''26	2.1 m	<i>g, r, U, B, V, I</i>

(Metzger 2017), albeit at lower sensitivity (a source as bright as GW170817 would be detected at  $\sim 20$  Mpc).

The first BNS detection of O3, LIGO/Virgo S190425z, was a single-detector event discovered by the Advanced LIGO-Livingston detector, with Virgo also observing at the time (LIGO Scientific Collaboration & Virgo Collaboration 2019f). Occurring at 2019 April 25 08:18:05 UTC, the estimated false alarm rate was 1 in 70,000 yr, with a high likelihood of being a BNS. The first reported BAYESTAR skymap provided an extremely coarse localization, resulting from the low signal-to-noise ratio in Advanced Virgo; it spanned  $\sim 10,000$  deg<sup>2</sup>, which is nearly a “pi of the sky.” The updated LALInference skymap (LIGO Scientific Collaboration & Virgo Collaboration 2019g), released at 2019 April 26 15:32:37 UTC, reduced the localization region requiring coverage by  $\approx 25\%$  to  $\sim 7500$  deg<sup>2</sup>. The all-sky averaged distance to the source is  $156 \pm 41$  Mpc.

In this Letter, we describe an  $\sim 8000$  square degree search for the KN counterpart to a single-detector GW event. Our campaign emphasizes the key role played by both large FOV telescopes like ZTF and Palomar Gattini-IR, as well as the associated follow-up systems. We demonstrate that our strategy for tiling the sky, vetting candidates, and pursuing follow-up is robust, and capable of promptly reducing 338,646 transient alerts from ZTF to a handful of interesting candidates for follow-up. Our Letter is structured as follows. We describe our observing plan in Section 2. The identified candidates, including their follow-up, are detailed in Section 3. We summarize our conclusions and future outlook in Section 4.

## 2. Observing Plan

Because S190425z came during Palomar night-time (2019 April 25 08:18:05 UTC), it occurred concurrently with ongoing survey observations by both ZTF and Palomar Gattini-IR. Within the 90% localization, approximately 44% of the original BAYESTAR map was observable from Palomar over the whole night, corresponding to  $\approx 5000$  deg<sup>2</sup>. The GW event was automatically ingested into the GROWTH ToO Marshal, a database that we specifically designed to perform target-of-opportunity follow-up of events localized to large sky-error regions, including GW, neutrino, and gamma-ray burst events (Coughlin et al. 2019a). Among several other features, the ToO marshal allows us to directly trigger the telescope queue for certain facilities to which GROWTH has access, namely ZTF, Palomar Gattini-IR, DECam, Kitt Peak EMCCD Demonstrator (KPED) on the Kitt Peak 84-inch telescope (Coughlin et al. 2019d), the Lulin One-meter Telescope (LOT) in Taiwan, and the GROWTH-India telescope<sup>42</sup> (V. Bhalerao et al. 2019, in preparation). We provide a brief description of each instrument in Table 1.

<sup>42</sup> <https://sites.google.com/view/growthindia/>

Triggering ToO observations for survey instruments like ZTF and Palomar Gattini-IR halts their ongoing survey observations and redirects them to observe only certain fields as directed by an observation plan. The observation plan generated by the ToO marshal relies on `gwemopt` (Coughlin et al. 2018a, 2019c), a code that optimizes the telescope scheduling process for GW follow-up. `gwemopt` handles both synoptic and galaxy-targeted search strategies; we employed the former to conduct observations with some of our facilities, Palomar Gattini-IR, GROWTH-India and ZTF, and the latter for scheduling observations with KPED. The coverage for both ZTF and Palomar Gattini-IR is shown in Figure 1, and the limiting magnitudes as a function of time in Figure 2.

### 2.1. ZTF

Serendipitously, after the BNS merger time and before the GW alert was distributed, ZTF had already observed 1920 deg<sup>2</sup> of the sky in the *r*-band, corresponding to  $\sim 19\%$  of the initial BAYESTAR map and  $\sim 12\%$  of the LALInference map. This overlap between ongoing survey observations and the LIGO-Livingston-only localization is unsurprising as both of the Advanced LIGO interferometers have maximum sensitivity in the sky overhead in North America (Finn & Chernoff 1993; Kasliwal & Nissanke 2014).

ZTF triggered ToO observations lasting three hours starting at 2019 April 25 09:19:07.161 UT, one hour after the trigger time. On night 1, our observing strategy involved a sequence of *g-r-g* band exposure blocks; each exposure was 30 s, with a typical depth of 20.4 mag, which is the normal duration of exposures during ZTF survey operation. The *g-r-g* sequence is the baseline observing strategy for GW follow-up with ZTF as it is specifically designed to capture the inter- and intra-night color evolution of GW170817-like KNe and to distinguish them from supernovae (Kilpatrick et al. 2017; Shappee et al. 2017). Due to the size of the localization, we obtained a *g-r* sequence, requiring references for each scheduled field. In addition, we required a 30 minutes gap between observations in *g* and *r* to avoid asteroids. Accounting for the loss in probability due to chip gaps and the processing success, ZTF covered 3250 deg<sup>2</sup>, corresponding to about 36% of the initial BAYESTAR and 19% of the LALInference maps on night 1.

Motivated by the increase in available observation time ( $\sim 5$  more hours than the first night), we modified our strategy on night 2 by taking longer integrations of 90 s each, corresponding to an average depth of 21.0 mag. We obtained one epoch in each of *g*- and *r*-band, corresponding to about 46% probability in the initial BAYESTAR or 21% of the LALInference maps.

After our observations on both nights were complete, a new LALInference skymap was released at 2019 April 26 14:51:42

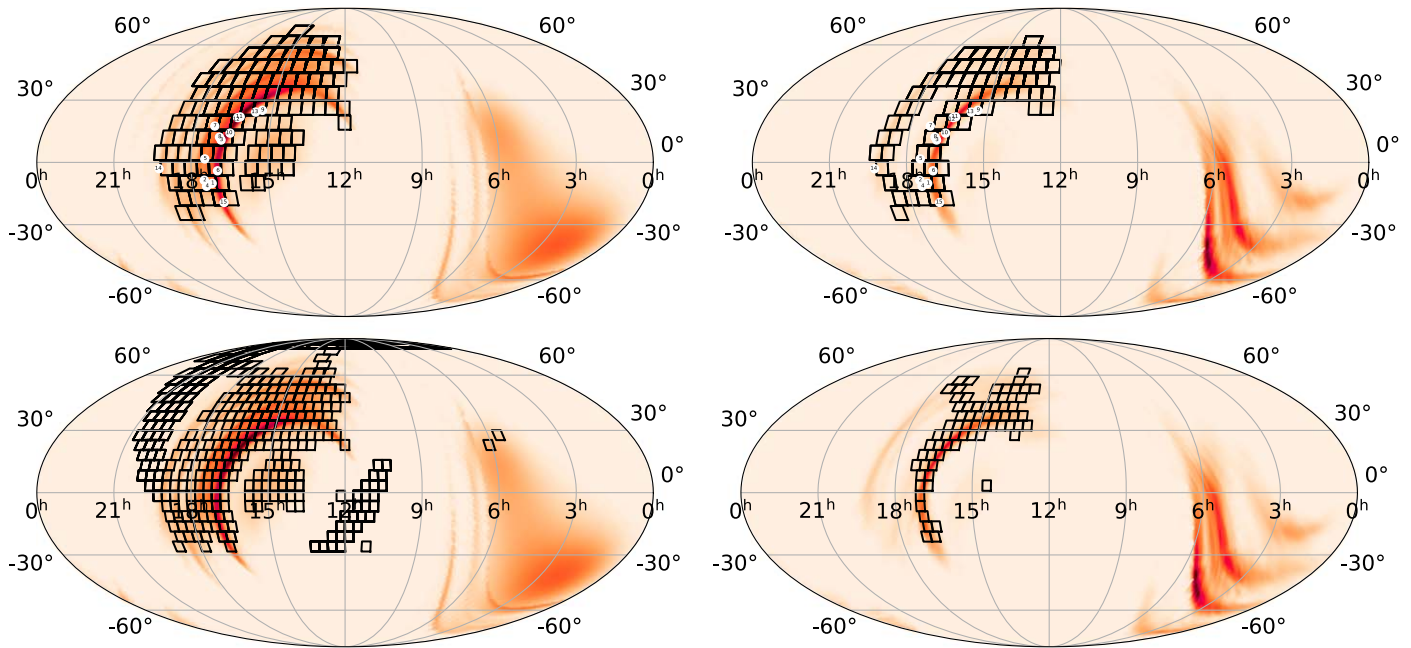


**Figure 1.** Coverage of S190425z. Left: the top and bottom rows show the  $\approx 47 \text{ deg}^2$  ZTF tiles and the  $\approx 25 \text{ deg}^2$  Palomar Gattini-IR tiles, respectively, on the 90% probability region of the initial BAYESTAR skymap, along with the identified transients highlighted in Table 3. For the ZTF observations, the numbering scheme is 1: ZTF19aarykkb, 2: ZTF19aarzaod, 3: ZTF19aasckwd, 4: ZTF19aasfogv, 5: ZTF19aasejil, 6: ZTF19aaryxfj, 7: ZTF19aascxux, 8: ZTF19aasdajo, 9: ZTF19aasbamy, 10: ZTF19aasckkq, 11: ZTF19aarycuy, 12: ZTF19aasbphu, 13: ZTF19aasbau, 14: ZTF19aarxxwb, 15: ZTF19aashlts. Right: tilings of the two telescopes on the final LALInference map. We only include the tiles in the inner 90% probability region for each skymap.

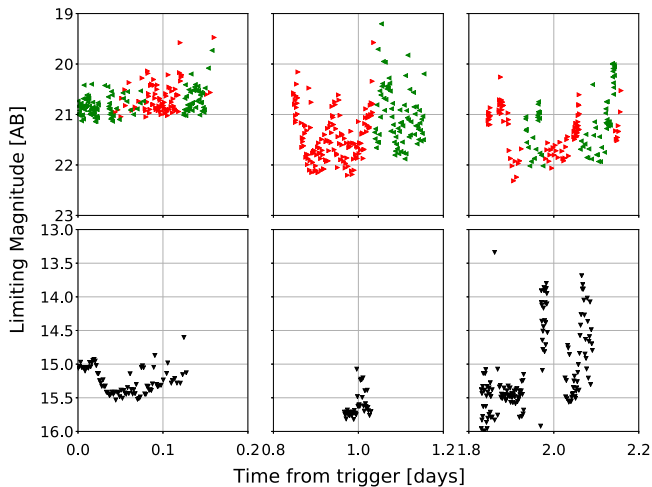


**Figure 2.** Limiting magnitude as a function of time for S190425z. On the top row is ZTF, while the bottom row is Palomar Gattini-IR, with the left, middle, and right panels corresponding to observations on the first, second, and third nights, respectively. The red and green triangles correspond to the  $r$ - and  $g$ -band limits from ZTF, while the black triangles correspond to the  $J$ -band limits from Palomar Gattini-IR.

UT (LIGO Scientific Collaboration & Virgo Collaboration 2019h). The LALInference runs reduced the skymap to  $\sim 7500 \text{ deg}^2$  and shifted more of the probability to two lobes near the Sun and in the Southern hemisphere (see Figure 1). In summary, ZTF covered about  $8000 \text{ deg}^2$  within the 99% integrated probability region within its two nights of observations. This corresponds to 46% of the probability in the original BAYESTAR skymap and 21% of the probability in the LALInference skymap. Our observations with ZTF over the two nights covered a  $5\sigma$  median depth of  $m_{\text{AB}} = 21.0$  in  $r$ -band and  $m_{\text{AB}} = 20.9$  in  $g$ -band.

## 2.2. Palomar Gattini-IR

Palomar Gattini-IR initiated ToO observations of the localization region at 2019 April 25 09:12:09 UT, 11 minutes after the initial notice time. The synoptic tiling strategy was determined in the same way as for ZTF (Coughlin et al. 2018a). Palomar Gattini-IR imaged a total of  $2401 \text{ deg}^2$  of the localization region spread over 227 field tiles, covering 32% of the probability region of the BAYESTAR skymap and 19% for the LALInference localization. Each field visit consisted of a sequence of eight dithered exposures of 8.1 s each, amounting to a total exposure time of 64.8 s per field. This resulted in a median stacked depth of  $m_{\text{AB}} = 15.5$  in  $J$ -band. The real-time data reduction pipeline (K. De et al. 2019, in preparation) reduced the data and identified transient candidates through the application of difference imaging using reference images of the fields.

## 2.3. Galaxy-targeted Follow-up

In addition to the synoptic surveys for counterparts, a subset of the available systems performed galaxy-targeted follow-up. This strategy was used by a number of teams to observe GW170817 (Arcavi et al. 2017b; Coulter et al. 2017; Valenti et al. 2017). The galaxy-targeted follow-up program relies on the Census of the Local Universe catalog (Cook et al. 2019); it is complete to 85% in star formation and 70% in stellar mass at 200 Mpc. The sky area coverage of galaxies is  $\approx 1\%$  within these local volumes (Cook et al. 2019). This makes targeted galaxy pointing tractable for small FOV telescopes (see Arcavi et al. 2017a or Golkhou et al. 2018 for example). Of the galaxies within the volume, our work prioritizes them for follow-up as follows.

The GROWTH ToO Marshal uses an algorithm modified from LCO's galaxy-targeted follow-up of GW events (Arcavi et al. 2017a), which uses a combination of a galaxy's location

in the GW localization region (including the distance),  $S_{\text{loc}}$ , the galaxy’s absolute  $B$ -band luminosity,  $S_{\text{lum}}$ , and the likelihood of detecting a counterpart at the galaxy’s distance  $S_{\text{det}}$ . We define  $S_{\text{det}}$  as a prioritization of a transient’s potential brightness, taking a fiducial limiting magnitude,  $m_{\text{lim}}$ , for the exposures of  $m_{\text{AB}} = 22$ , and convert it to a limiting apparent luminosity  $L_{\text{lim}}$ . We also compute the luminosity for a potential transient with an absolute magnitude between  $-12$  and  $-17$ , using wide bounds to be robust against differences in intrinsic brightness. Then,  $S_{\text{det}}$  becomes  $S_{\text{det}} = \frac{L_{\text{KNmax}} - L_{\text{KNmin}}}{L_{\text{KNmax}} - L_{\text{lim}}}$ , which we limit to be between 0.01 and 1. Our final metric is therefore  $S = S_{\text{loc}} \times S_{\text{lum}} \times S_{\text{det}}$ .

Beginning 4 hr after the event, LOT observed 85 galaxies in the initial 90% localization (Tan et al. 2019a, 2019b). LOT used 180 s exposures in  $R$ -band with seeing varying between  $1''.5$  and  $2''.5$ . Using comparisons to Pan-STARRS images, these exposures yielded a typical  $5\sigma$  limiting magnitude of  $m_{\text{AB}} = 20$ . Similarly, KPED started the galaxy-targeted follow-up 1.9 hr after the merger and continued until the first ZTF candidates came online. KPED imaged 10 galaxies in the  $r$ -band filter for 300 s, finding no visible transients up to  $r = 20.8$  (Ahumada et al. 2019a). 300 s is the fiducial time chosen for KPED to potentially reach limiting magnitudes of  $m_{\text{AB}} = 22$ , useful for both the transient discovery and follow-up (Coughlin et al. 2019d).

### 3. Candidates

We now briefly describe the candidate filtering criteria for the ToO program for ZTF and Palomar Gattini-IR (see Coughlin et al. 2019a for further details). For GROWTH-India, LOT, and KPED, we did not identify any viable counterparts without previous history of variability in the analysis.

#### 3.1. Candidates from ZTF

A ZTF transient alert is defined as a  $5\sigma$  change in brightness in the image relative to the reference epoch. For ZTF, all transient alerts flagged for follow-up required at least two detections separated by 15 minutes in order to remove asteroids and other transient objects. We used the Pan-STARRS1 point source catalog (PS1 PSC; Tachibana & Miller 2018) to remove candidates located less than  $2''$  from likely point sources (i.e., stars). Full details on the PS1 PSC can be found in Tachibana & Miller (2018); briefly, the authors build a machine learning model that determines the relative likelihood that a PS1 source is a point source or extended based on PS1 colors and shape measurements. The model is trained using sources observed with the *Hubble Space Telescope*, achieving an overall accuracy of  $\sim 94\%$ , and classifying  $\sim 1.5 \times 10^9$  total sources.

We also used a real-bogus (RB) classifier to remove common image subtraction artifacts (Mahabal et al. 2019). This method consists of a random forest classifier trained with real objects and artifacts from ZTF images, separating objects with an accuracy of  $\sim 89\%$ . In order to capture the majority of real events, the threshold was set to  $\text{RB} > 0.25$ . In addition, the transients must have brightened relative to the reference image, leading to a positive residual after the image subtraction. Furthermore, the program excluded all objects within  $20''$  of  $m_{\text{AB}} < 15$  stars to avoid artifacts from blooming, thus excluding  $\sim 2\%$ – $5\%$  of the imaged region, which depends

**Table 2**  
Filtering Results for Both ZTF Nights

Filtering Criteria	# of Alerts on April 25	# of Alerts on April 26
ToO alerts	50,802	287,844
Positive subtraction	33,139	182,095
Real	19,990	118,446
Not stellar	10,546	61,583
Far from a bright source	10,045	58,881
Not moving	990	5815
No previous history	<b>28</b>	<b>234</b>

**Note.** The quantities represent the number of alerts that passed a particular step in the filter. Each step is run over the remaining alerts from the previous stage. The criteria are described in Section 3.1 and the total number of relevant candidates is highlighted. In particular, “Real” indicates an RB score greater than 0.25, and “not moving” indicates that there are more than two detections separated by at least 30 minutes. The bold values refer to the final number of candidates remaining after our initial filter process.

significantly on stellar density.<sup>43</sup> The final step involved constraining the search to events that have no historical detections prior to three days before the trigger.

This filtering scheme reduced the number of ZTF alerts from 50802 to 28 for the first night and from 287844 to 234 relevant candidates for the second night. A more detailed breakdown on the number of alerts that successfully met the criteria at each filtering step can be found in Table 2.

The candidates that passed these criteria were filtered and displayed by the GROWTH Marshal (Kasliwal et al. 2019b), a database used to display historical lightcurves (including upper limits) for each object that also performs cross-matches with external catalogs. We subjected each of the remaining candidates to a thorough human vetting process to determine whether the transient could be a viable counterpart to S190425z. Through this vetting process, we removed candidates whose coordinates were outside the 90% contour in the GW localization, and candidates that had archival detections in the Pan-STARRS1 Data Release 2 (Flewelling 2018). We flagged active galactic nuclei based on the *WISE* colors (Wright et al. 2010) for each transient and its offset from the nucleus of the galaxy. Furthermore, we prioritized candidates whose photometric/spectroscopic redshift was consistent with the GW distance estimate, and whose extinction-corrected light curve exhibited rapid color evolution initially. For the most promising candidates in our vetted list, we performed forced photometry at the position of the source to ensure that there were no historical detections with ZTF.

Our first night of observations yielded only two such candidates that passed both the automatic filtering and human vetting processes. These two candidates were ZTF19aarykbb and ZTF19aarzaod. The second night of observations allowed us to identify additional candidates detected on the first night that were consistent with the new skymap, thereby increasing our candidate list from two to 13 from the first night to the second. We describe the most promising of these 15 candidates in more detail in Section 3.3.

<sup>43</sup> Estimates of the amount of excluded area rely on the assumption that the sky fraction excluded around  $m_{\text{AB}} < 15$  stars, within a few circular regions of  $1 \text{ deg}^2$  in the skymap that we checked, is representative of the overall sky fraction excluded from the entire imaged region.

**Table 3**

Follow-up Table for the Palomar Gattini-IR Candidate Described in Section 3.2 and the 15 Most Interesting ZTF Candidates from Kasliwal et al. (2019c) and Anand et al. (2019)

Candidate	Coordinates (R.A., Decl.)	Discov. Mag.	Classification	Spec. Facilities	Phot. Evol.	Redshift/Host
ZTF19aarykkb	17:13:21.95 −09:57:52.1	$r = 18.63$	SNII $z = 0.024$	HCT, LT, DCT	...	0.024 (s)
ZTF19aarzaod	17:31:09.96 −08:27:02.6	$r = 20.11$	SNIIn $z = 0.028$	SALT	...	0.028 (s)
ZTF19aasckwd	16:52:39.45 +10:36:08.3	$r = 20.15$	SN Ia $z = 0.145$	SOAR	...	0.15 (s)
ZTF19aasckkq	16:33:39.14 +13:54:36.7	$g = 20.86$	SN Iib $z = 0.052$	P200, SOAR	...	0.053 (s)
ZTF19aasbphu	16:22:19.95 +21:24:29.5	$r = 19.71$	Nuclear*	...	0.11	0.0971 (p)
ZTF19aaryxjf	16:58:22.87 −03:59:05.1	$g = 19.95$	SN*	...	−0.014	0.07791 (s, GLADE)
ZTF19aarxxwb	19:14:46.40 −03:00:27.0	$g = 18.89$	SN*	...	0.12	hostless
ZTF19aasdajo	16:57:25.21 +11:59:46.0	$g = 20.7$	SN*	...	0.045	0.292 (p)
ZTF19aasbamy	15:25:03.76 +24:55:39.3	$g = 20.66$	SN*	...	0.01	0.201 (p)
ZTF19aarycuy	16:16:19.97 +21:44:27.4	$r = 20.07$	SN*	...	0.02	0.127 (p)
ZTF19aasbau	15:40:59.91 +24:04:53.8	$g = 20.49$	SN*	...	0.01	0.04 (s, CLU)
ZTF19aasejil	17:27:46.99 +01:39:13.4	$g = 20.53$	SN*	...	0.01	0.199 (p)
ZTF19aascxux	17:13:10.39 +17:17:37.9	$g = 20.56$	SN*	...	0.06	0.165 (p)
ZTF19aashlts	16:52:45.01 −19:05:38.9	$r = 19.95$	SN*	...	0.03	hostless
ZTF19aasfogv	17:27:22.32 −11:20:01.9	$g = 20.53$	SN*	...	0.01	hostless

**Note.** The sources with a star (\*) have photometric evolution (in units of mag/day) that is inconsistent with the evolution of a KN (Section 3.3). Spectra obtained with SOAR (Nicholl et al. 2019) were critical in classifying ZTF19aasckwd and ZTF19aasckkq while spectra from SALT (Buckley et al. 2019) allowed the classification of ZTF19aarzaod. GROWTH teams acquired spectra of ZTF19aarykkb with HCT, LT, and DCT (Dichiara et al. 2019; Pavana et al. 2019; Perley et al. 2019a) and also provided useful photometric data toward the classification of these transients (Ahumada et al. 2019a, 2019b; Bhalariao et al. 2019; Perley et al. 2019b; Tan et al. 2019b). We monitored the transients on average for seven days. The redshift, spectroscopic (s) or photometric, (p) of the host galaxy is also listed.

To double-check that we did not miss any candidates, we used Kowalski,<sup>44</sup> an open-source system used internally at Caltech (primarily) to archive and access ZTF’s alerts and light curves (Duez et al. 2019). Specifically, we used Kowalski’s web-based GUI called the ZTF Alert Lab, with which users can efficiently query, search, and preview alerts. Our results were consistent with the results above. To triple-check that we did not miss any candidates, we also carried out an additional automatic search of the AMPEL alert archive (Nordin et al. 2019) for transients that might have escaped. No additional candidates from either night were found.

### 3.2. Candidates from Palomar Gattini-IR

For Palomar Gattini-IR, we adopted the following selection criteria for human vetting of sources identified in the difference imaging.

1. We selected candidates that were at least  $1'$  away from bright stars with  $m_j < 10$ , excluding  $\sim 0.7\%$ – $2\%$  of the imaged region, in order to remove contamination from subtraction artifacts.<sup>45</sup>
2. The first detection of the candidate must have been after the GW trigger time.
3. An object must have at least two detections with a signal-to-noise ratio greater than 5 or a signal-to-noise ratio greater than 7 in one detection. Among sources with single detections, we also rejected known asteroids.

No viable counterparts were identified in this search.

<sup>44</sup> <https://github.com/dmitryduez/kowalski>

<sup>45</sup> Estimates of the amount of excluded area rely on the assumption that the sky fraction excluded around  $m_{AB} < 10$  stars, within a few circular regions of  $1 \text{ deg}^2$  in the skymap that we checked, is representative of the overall sky fraction excluded from the entire imaged region.

### 3.3. Follow-up of ZTF Candidates

The 15 sources that were identified from ZTF observations are shown in Table 3 and on Figure 1. Using a variety of resources including the spectral energy distribution (SED) Machine (SEDM; Blagorodnova et al. 2018; Rigault et al. 2019) on the Palomar 60 inch (P60) telescope, the Double Beam Spectrograph (DBSP; Oke & Gunn 1982) on the Palomar 200 inch (P200) telescope, the Robert Stobie Spectrograph (RSS; Smith et al. 2006) on the Southern African Large Telescope (SALT), the Liverpool telescope (LT; Steele et al. 2004), the GROWTH-India telescope, the KPED, the Himalayan Chandra Telescope (HCT), the Discovery Channel Telescope (DCT), and LOT, we followed up each of these candidates with further photometry and/or spectroscopy.

A total of five objects were classified using spectroscopy (Buckley et al. 2019; Nicholl et al. 2019; Perley et al. 2019a) and we tracked the color evolution of 15 objects using photometry for about seven days on average. A KN is expected to show a rapid evolution in magnitude (Metzger 2017); GW170817 faded  $\Delta r \sim 1$  mag per day over the first three days and by  $\Delta r \sim 4.2$  mag total around day 10. Thus, we can use photometric light curves to determine whether a transient is consistent with the expected evolution for a KN. Some photometrically monitored transients showed evolution that was too slow ( $\Delta r \sim 0.1$  mag per day) to be consistent with GW170817 or KN model predictions. Many other candidates highlighted in Kasliwal et al. (2019c) were observed with GROWTH facilities; however, they were later excluded by the updated LALInference skymap. In addition to these sources, we reported objects in Kasliwal et al. (2019c) with ZTF detections before the event time to the community in order to limit the number of false positives identified by other surveys that may not have recently imaged those areas of the sky.

We now provide a broad summary of the most promising candidates ruled out by spectroscopy, as examples of the follow-up performed by the GROWTH facilities when vetting candidates.

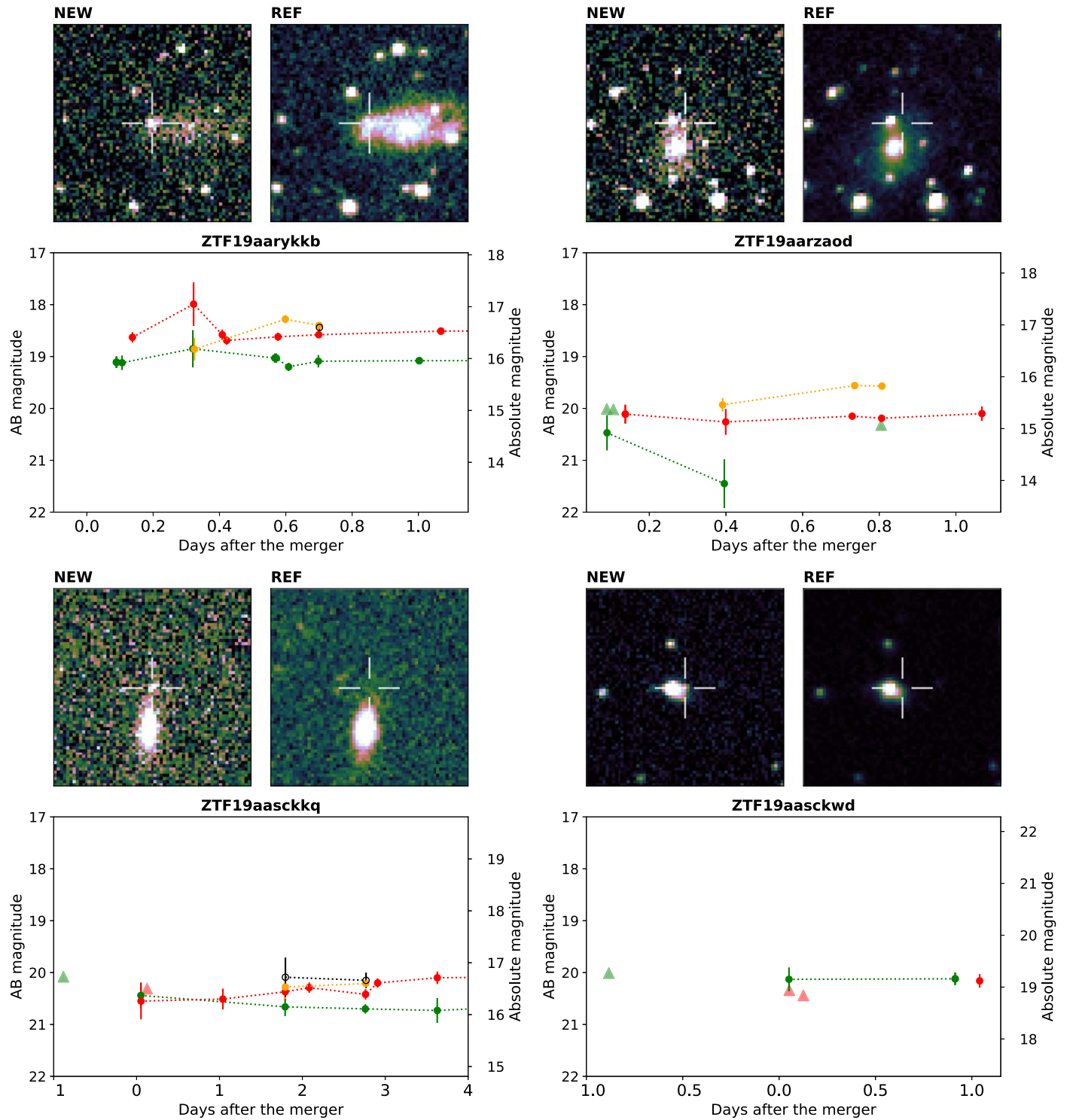


**Figure 3.** Light curves and *r*-band cutouts for the ZTF candidates discussed in Section 3.3. The light curves are constructed with data acquired with GROWTH facilities: for ZTF19aarykbb, the data is from ZTF, LOT, GIT, and LT; for ZTF19aarzaod, ZTF, LOT, and LT; for ZTF19aasckkq, ZTF, KPED, and LT; and for ZTF19aasckwd, ZTF and KPED. We used colors to represent each band in the light curves: green for *g*-band, red for *r*-band, yellow for *i*-band, and black for *z*-band. While triangles in the light curve represent upper limits, filled circles are the magnitudes of the object. For each transient, the cutout on the left corresponds to the ZTF discovery image and the right cutout corresponds to the ZTF reference image of the host. A cross marks the location of the transient in the reference image. The cutouts are 0.7 sq. arcmin with north being up and east to the left.

In particular, we highlight the light curves of ZTF19aarykbb, ZTF19aarzaod, ZTF19aasckkq, and ZTF19aasckwd in the top-left, top-right, lower-left and lower-right panels, respectively, in Figure 3 and discuss them briefly below. The associated spectra

are shown in the top panel of Figure 5; the spectrum of ZTF19aasckwd is not shown as we only have a spectrum of the galaxy host. We used the value of  $H_0 = 67.4 \text{ km s}^{-1} \text{ Mpc}^{-1}$  (Aghanim et al. 2018) to calculate absolute magnitudes.

### 3.3.1. ZTF19aarykkb

We first detected the transient ZTF19aarykkb 2.13 hr after the merger and highlighted it in the first ZTF GCN (Kasliwal et al. 2019c). ZTF19aarykkb is  $12''1$  offset from the host galaxy, which is at a redshift of  $z = 0.024$ , corresponding to a luminosity distance of 106 Mpc. The absolute magnitude of the discovery is  $g = -15.9$ , which is broadly consistent with GW170817 and KNe predictions. We ran forced photometry in archival ZTF images of the region, finding no variability at the coordinates before the merger. The last upper limit at this location was 5.8 days before the LVC alert in  $g$ -band ( $m_{AB} > 18.74$  in  $g$ -band). Due to its distance and discovery mag, several facilities followed up this source (Burke et al. 2019; Chang et al. 2019a; Dichiaro et al. 2019; Morihana et al. 2019a; Nicholl et al. 2019; Perley et al. 2019a; Rhodes et al. 2019). The LOT group in Taiwan imaged the object 6 hr after the transient set in Palomar (Tan et al. 2019b); later that day, the LT continued the monitoring. This object was imaged 18 times within the first 26 hr after the merger. The first spectrum for this object came from the Himalayan Chandra Telescope (HCT) about 10.67 hr after the trigger (Pavana et al. 2019), showing a strong  $H\alpha$  line at a redshift of  $z = 0.024$ . This was confirmed 8 hr later by the LT team with the Spectrograph for the Rapid Acquisition of Transients (SPRAT; Piascik et al. 2014), who classified it as a young SN Type II (Perley et al. 2019a), based on the characteristic P-Cygni profile in the LT spectrum. An additional spectrum was taken about 10 hr later with the DeVeney spectrograph mounted on the 4.3 m DCT (Dichiaro et al. 2019), showing similar strong  $H\alpha$ , furthermore confirming the SN classification (see Figure 5).

### 3.3.2. ZTF19aarzaod

ZTF19aarzaod was first detected by ZTF 2.15 hr after the merger (Kasliwal et al. 2019c) with its last upper limit ( $m_{AB} > 20.01$  in  $g$ -band) six days prior the merger. Forced photometry did not show previous history of variability at the transient location. The redshift of the host galaxy is  $z = 0.028$ , putting the transient at a distance of 128.7 Mpc. The transient is offset by  $8''2$  from the host galaxy and its absolute magnitude at discovery was  $r = -15.3$ , which is also consistent with a GW170817-like KN. ZTF19aarzaod was extensively followed up with various observatories (Buckley et al. 2019; Castro-Tirado et al. 2019; Hiramatsu et al. 2019; Izzo et al. 2019; Morihana et al. 2019a; Nicholl et al. 2019; Rhodes et al. 2019; Wiersema et al. 2019) and was imaged 13 times during the first day. Spectroscopic observations of ZTF19aarzaod were taken with RSS mounted on SALT on UT 2019 April 26.0 under a special GW follow-up program 2018-2-GWE-002 and reduced with a custom pipeline based on PyRAF routines and the PySALT package (Crawford et al. 2010). The spectrum covered a wavelength range of 470–760 nm with a spectral resolution of  $R = 400$ . The spectrum shows broad  $H\alpha$  emission along with some He I features (see Figure 5) classifying it as a type II supernova at  $z = 0.028$  (Buckley et al. 2019).

### 3.3.3. ZTF19aasckkq

The transient ZTF19aasckkq (Anand et al. 2019) was first detected by ZTF 1.23 hr after the merger. It is offset from the host galaxy by  $10''1$ , and its last upper limit ( $m_{AB} > 20.1$  in  $g$ -band) was the night before the merger. We ran forced

photometry at the location of the transient, finding no activity before the merger. The discovery absolute mag is  $r = -16.3$ , similar to GW170817 at peak. ZTF19aasckkq was followed up 18 hr after the last ZTF detection by LT and KPED (Ahumada et al. 2019b). This transient was imaged 16 times for a period of 3.8 days by a variety of observing groups (Ahumada et al. 2019b, 2019c; Perley et al. 2019b, 2019c). Nicholl et al. (2019) first classified ZTF19aasckkq as a Type IIb SN at  $z \sim 0.05$ , which is consistent with the galaxy redshift (Hosseinzadeh et al. 2019). In Figure 5, we highlight the presence of He I,  $H\alpha$ , and  $H\beta$  absorption features in the first spectrum we acquired with P200+DBSP, confirming its classification as a SN IIb at a redshift of  $z = 0.0528$ . The source was still bright at  $r = 19.8$ , 14 days after S190425z.

### 3.3.4. ZTF19aasckwd

ZTF19aasckwd was detected 1.23 hr after the merger about  $4''2$  from its host galaxy (Anand et al. 2019). Its last upper limit ( $m_{AB} > 20.1$  in  $g$ -band) was the night before the trigger. The forced photometry search did not show activity prior to the merger. This transient was imaged five times during the first 24 hr and it was classified as a SN Ia by Nicholl et al. (2019) at a redshift of  $z = 0.145$  (Hosseinzadeh et al. 2019). The absolute magnitude at discovery was  $r = -19.2$ , a few magnitudes brighter than what is expected from a KN.

## 3.4. Follow-up of Non-ZTF Candidates

Here, we report on the follow-up triggered by the GROWTH team of a number of transients discovered by other facilities to be consistent with the LALInference skymap. We queried the GROWTH follow-up marshal at the positions of the most promising transients announced in order to determine whether (1) the transient had historical detections with ZTF, or (2) our concurrent photometry of the object also supported the KN hypothesis. Additionally, we used LT, GROWTH-India Telescope, and DECam to obtain photometry of the candidates that were not detected with ZTF because they were either fainter than the ZTF average upper limits or inaccessible due to their sky location. Table 4 summarizes the most relevant non-GROWTH objects followed up by the GROWTH collaboration, and we briefly discuss them below.

### 3.4.1. Swift's Ultraviolet/Optical Telescope (UVOT) Candidate

We followed up photometrically the *Swift*/UVOT candidate (Breeveld et al. 2019), discovered at R.A. = 17:02:19.2, decl. =  $-12:29:08.2$  in  $u$ -band with  $m_{Vega} = 17.7 \pm 0.2$ . The transient was within a few hundred arcseconds of two galaxies within the localization volume. After its initial detection with *Swift*, several other facilities (Andreoni et al. 2019b; Arcavi et al. 2019; Breeveld et al. 2019; Chang et al. 2019b; De et al. 2019; Hu et al. 2019; Im et al. 2019; Kann et al. 2019; Kong et al. 2019; Morihana et al. 2019b; Shappee et al. 2019; Tanvir et al. 2019; Troja et al. 2019; Waratkar et al. 2019), including ZTF and Palomar Gattini-IR, reported non-detections or pre-discovery upper limits that indicated the transient might be rapidly fading in the ultraviolet. Palmese et al. (2019) reported an object offset by  $<1''$  from the position of the reported UVOT candidate after visually inspecting archival DECam optical images. Using the GROWTH-DECam program, Bloom et al. (2019) detected a source that is consistent with the coordinates reported by Palmese et al.



**Table 4**  
GROWTH Follow-up Table for Candidates Reported by Other Surveys

Candidate	Coordinates (R.A., Decl.)	Discovery Mag.	GROWTH Follow-up	Upper Limits
UVOT	17:02:19.21 –12:29:08.2	$u = 17.74$	GIT, LOT, DECam	DECam $g > 24.0$
...	...	...	...	DECam $r > 24.0$
...	...	...	...	DECam $i > 23.7$
...	...	...	...	DECam $z > 23.1$
AT2019ebq-PS19qp	17:01:18.33 –07:00:10.4	$i = 20.40$	Keck spectrum SN Ib/c	...
Gaia19bpt	14:09:41.88 +55:29:28.1	$o = 18.49$	ZTF19aarioci (4.12)	...
AT2019ebu-PS19pp	14:19:49.43 +33:00:21.7	$i = 20.77$	ZTF19aasbgll (2.10)	$r = 20.60$
AT2019ebw-PS19pq	15:02:17.02 +31:14:51.6	$i = 20.92$	ZTF19aasazok (11.95)	$g = 20.91$
AT2019ecc-PS19pw	15:26:29.53 +31:39:47.5	$i = 20.10$	ZTF19aapwpgg (17.96)	$r = 20.14$
AT2019eck-PS19qe	15:44:24.53 +32:41:11.0	$i = 20.81$	ZTF19aapfrw (24.97)	$g = 20.13$
AT2019ecl-PS19qg	15:48:11.85 +29:12:07.1	$i = 20.51$	ZTF19aasgwnp (25.89)	$g = 21.02$
AT2019ebr-PS19qj	16:35:26.48 +22:21:36.4	$i = 19.79$	ZTF18aaoxrvr (25.86)	$g = 20.83$
AT2019ebo-PS19qn	16:54:54.71 +04:51:31.5	$i = 20.02$	ZTF19aarpgau (9.87)	$g = 20.40$
AT2019eao-ATLAS19hyo	13:01:18.63 +52:09:02.1	$o = 19.36$	LT	$g > 22.1$
AT2019ebn-ATLAS19hwh	13:54:47.42 +44:46:27.3	$o = 19.07$	LT	$g > 22.1$
AT2019ebm-ATLAS19hwn	12:59:58.58 +29:14:30.7	$o = 19.42$	LT	$g > 22.3$
AT2019ebl-ATLAS19hyx	14:32:31.53 +55:45:00.1	$o = 19.28$	LT	$g > 22.3$
AT2019dzv-ATLAS19hxm	14:01:45.02 +46:12:56.1	$o = 19.23$	LT	$g > 22.2$

**Note.** GROWTH-India, LOT, and DECam-GROWTH follow-up of the *Swift*/Ultraviolet/Optical Telescope (UVOT) candidate discovered by Breeveld et al. (2019) helped confirm its classification as a likely M-dwarf flare (Andreoni et al. 2019b; Arcavi et al. 2019; Bloom et al. 2019; Breeveld et al. 2019; Chang et al. 2019b; De et al. 2019; Hu et al. 2019; Im et al. 2019; Kann et al. 2019; Kong et al. 2019; Lipunov et al. 2019b; Morihana et al. 2019b; Palmese et al. 2019; Shappee et al. 2019; Tanvir et al. 2019; Troja et al. 2019; Waratkar et al. 2019). Our initial Keck spectrum of another promising candidate, AT2019ebq/PS19qp (Smith et al. 2019) showed it was a Type II SN (Jencson et al. 2019). Several of the PS1 candidates reported by Smith et al. (2019), as well as Gaia19bpt (Kostrzewa-Rutkowska et al. 2019) were found to have previous detections with ZTF (Andreoni & Bellm 2019; Coughlin et al. 2019b). For these sources, we list the number of days before S190425z that they were detected in parentheses. LT provided constraining upper limits of some reported ATLAS candidates (McBrien et al. 2019; Perley & Copperwheat 2019).

(2019), but no transient at the coordinates reported by *Swift* (Kong et al. 2019; see Table 4). The slight trailing observed in images of the original UVOT source (which introduced uncertainty in the astrometry) strongly hinted at the physical association between the transient and the offset source. The colors of the associated source ( $r - z = 1.53$  and  $g - r > 0.97$ ) are consistent with those of a M2-dwarf (West et al. 2011). For this reason, a likely explanation for the observed ultraviolet transient is that it was a galactic M2-dwarf flare (Bloom et al. 2019; Lipunov et al. 2019b), unassociated with the GW event. The photometry of the UVOT candidate is shown with a Sloan Digital Sky Survey (SDSS) spectra of a M2-dwarf in Figure 4.

### 3.4.2. AT2019ebq/PS19qp

We also obtained spectroscopy of AT2019ebq/PS19qp (Smith et al. 2019) with the Near-Infrared Echelle Spectrometer (NIRES) on Keck II. This candidate was initially claimed to be exceptional in that its optical spectrum taken with the Gran Telescopio Canarias (GTC) contained broad absorption features “unlike normal supernovae;” therefore Jonker et al. (2019) highlighted it as a promising KN candidate. Our near-IR spectrum taken  $\sim 1.5$  days after the trigger, however, exhibited broad P-Cygni SN-like features of He I that indicated that the transient was a Type Ib/c SN (Jencson et al. 2019), ruling out its association with S190425z (see the bottom panel of Figure 5). Several other facilities that also followed up this source helped verify its classification (Carini et al. 2019; Dimitriadis et al. 2019; Jencson et al. 2019; Lipunov et al. 2019a; McCully et al. 2019; Morokuma et al. 2019; Schady et al. 2019).

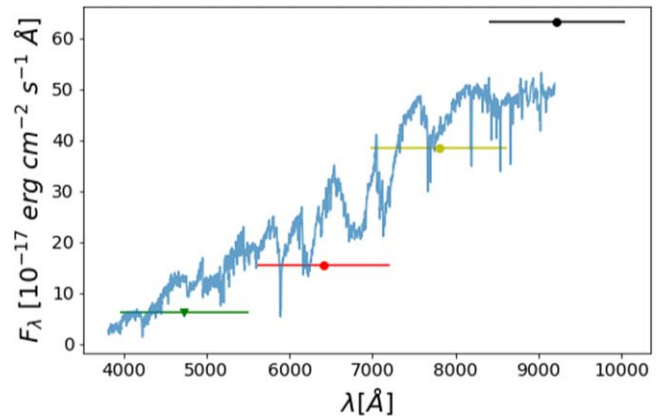


**Figure 4.** DECam ( $g$ ,  $r$ ,  $i$  and  $z$ -band) fluxes of the UVOT candidate discussed on Section 3.4.1 are over-plotted on the spectra of an SDSS M2-dwarf.

Seven additional PS1 candidates (out of the 20 transients reported by Smith et al. 2019) were ruled out based on previous ZTF detections (Andreoni et al. 2019a; see Table 4).

### 3.4.3. Marginal ATLAS Candidates

Additionally, we acquired a short sequence (40 s each in  $gri$  filters) of imaging at the locations of all five of the marginal ATLAS transients reported by McBrien et al. (2019) using IO: O (Steele et al. 2004) on the 2 m Liverpool Telescope (Perley & Copperwheat 2019). No significant source was detected at the location of any of them (to typical depths of 22 mag; see Table 4). Combined with the fact that none of these transients had a detectable host galaxy, this suggests these transients were

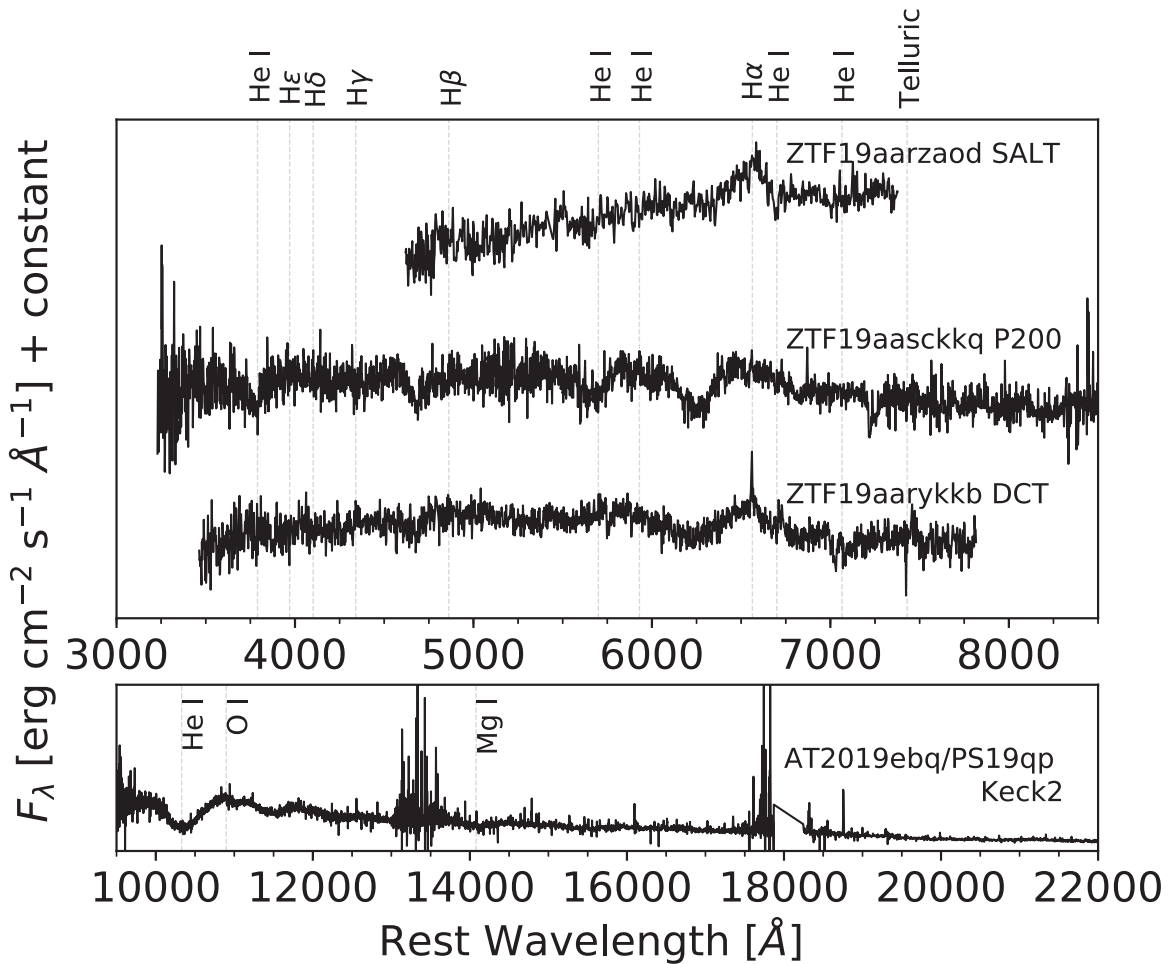


**Figure 5.** Spectra of all the candidates for which spectroscopic data were taken. The transient name and instrument used to obtain the spectrum are noted on the right-hand side of the plot. We show the spectrum for AT2019ebq/PS19qp in its own panel given the different wavelengths covered from the other transients. The dotted gray lines show the characteristic features in each spectrum that helped with its classification. These four transients were all classified as core-collapse SNe. The classification and phase for each transient is as follows: ZTF19aascckq—SN Iib, seven days; ZTF19aarykkb—SN II, one day (Dichiara et al. 2019); ZTF19aarzaod—SN II, zero days (Buckley et al. 2019); AT2019ebq/PS19qp—SN Ib/c, one day (Jencson et al. 2019).

likely to be spurious or perhaps short-timescale flares from faint stars.

#### 4. Conclusions

In this Letter, we have described the first follow-up of a binary neutron star event with ZTF and Palomar Gattini-IR. Covering more than 8000 deg<sup>2</sup> with ZTF and 2400 deg<sup>2</sup> with Palomar Gattini-IR over two nights, we show how these systems in combination with follow-up facilities are capable of rapidly identifying and characterizing transients on hour to day timescales over sky regions of this size. We show how it is possible to reduce 338,646 alerts to 15 previously unidentified candidate counterparts. We also show how with the follow-up resources available to GROWTH, we can rule out these objects as viable candidates.

Assuming an optical/near-IR counterpart with a luminosity similar to that of GW170817, which had an absolute magnitude of about  $-16$  in  $g$ -,  $r$ -, and  $J$ -bands, the apparent magnitude in these bands for the distribution of distances to S190425z is  $m_{AB} \approx 19$ – $20.5$ . This varies between 1 mag brighter than to near the detection limit for ZTF for this analysis, indicating ZTF is well primed for detecting a GW170817-like source at these distances. We expect that a closer or brighter than

expected source (GW170817 would be detected at  $\sim 20$  Mpc) should be detectable with Palomar Gattini-IR.

As a cross-check of the number of sources that we are identifying, we compare to the fiducial SN rate of  $\approx 10^{-4}$  Mpc<sup>-3</sup> yr<sup>-1</sup> (Li et al. 2011). The 90% localization volume of the GW skymap is  $\sim 2.1 \times 10^7$  Mpc<sup>3</sup>. As stated above, ZTF covered about 46% of the skymap, meaning that we expect to detect  $\sim 2.1 \times 10^7$  Mpc<sup>3</sup>  $\times 1.04 \times 10^{-4}$  Mpc<sup>-3</sup> yr<sup>-1</sup>  $\times 0.46 \approx 2.7$  day<sup>-1</sup>. Because the distribution of Type II SNe at peak luminosity falls between absolute magnitudes of  $\approx -15$  to  $-20$  mag (Richardson et al. 2014), brighter than the expected distribution at peak for KNE, our follow-up observations with ZTF should have detected all of the bright, and most of the dim Type II SNe. Having taken images for about 12 hr during the nights, we would expect to detect  $\sim 1$ – $2$ , which is consistent with the two young SNe highlighted in this Letter.

Going forward, prioritizing further automatized classification of objects can lead to more rapid follow-up and dissemination of the most interesting objects. For example, the inclusion of machine-learning-based photometric classification codes such as RAPID (Muthukrishna et al. 2019) will help facilitate candidate selection and prioritization. We are also actively improving the scheduling optimization, and have since added a

feature to schedule using the “secondary” ZTF grid, that is designed to fill in the chip gaps.

The follow-up of S190425z highlights two important points. The first is that rapid dissemination of updated GW sky maps is useful for tiling prioritization. This helps mitigate the effects of shifting localization regions, including potentially decreasing sky areas. The second is that we are capable of performing nearly all-sky searches with ZTF and Palomar Gattini-IR and conducting the necessary follow-up with partner facilities, even in the case of a single-detector GW trigger. This event serves to extend the frontier in searches for optical transients in large areas. The intermediate Palomar Transient Factory found optical counterparts to eight long GRBs localized to  $\sim 100 \text{ deg}^2$  (Singer et al. 2015), with GRB 130702A (Singer et al. 2013) being the first of its kind, and this event has shown it is possible to cover more than an order of magnitude larger sky area. One caveat to this conclusion is that in general, single-detector localizations will include regions on the sky that are not accessible to one ground-based facility alone; this motivates the use of coordinated networks of telescopes with worldwide coverage (Nissanke et al. 2013; Kasliwal & Nissanke 2014). However, we have demonstrated that the network on hand is capable of overcoming the challenges of rapidly and efficiently searching for electromagnetic counterparts in this new era of GW astronomy.

We would like to thank Peter Nugent for comments on an early version of this Letter.

This work was supported by the GROWTH (Global Relay of Observatories Watching Transients Happen) project funded by the National Science Foundation under PIRE grant No. 1545949. GROWTH is a collaborative project among California Institute of Technology (USA), University of Maryland College Park (USA), University of Wisconsin Milwaukee (USA), Texas Tech University (USA), San Diego State University (USA), University of Washington (USA), Los Alamos National Laboratory (USA), Tokyo Institute of Technology (Japan), National Central University (Taiwan), Indian Institute of Astrophysics (India), Indian Institute of Technology Bombay (India), Weizmann Institute of Science (Israel), The Oskar Klein Centre at Stockholm University (Sweden), Humboldt University (Germany), Liverpool John Moores University (UK) and University of Sydney (Australia).

Based on observations made with the Liverpool Telescope operated on the island of La Palma by Liverpool John Moores University in the Spanish Observatorio del Roque de los Muchachos of the Instituto de Astrofísica de Canarias with financial support from the UK Science and Technology Facilities Council. Based on observations obtained with the Samuel Oschin Telescope 48 inch and the 60 inch Telescope at the Palomar Observatory as part of the Zwicky Transient Facility project. ZTF is supported by the National Science Foundation under grant No. AST-1440341 and a collaboration including Caltech, IPAC, the Weizmann Institute for Science, the Oskar Klein Center at Stockholm University, the University of Maryland, the University of Washington, Deutsches Elektronen-Synchrotron and Humboldt University, Los Alamos National Laboratories, the TANGO Consortium of Taiwan, the University of Wisconsin at Milwaukee, and Lawrence Berkeley National Laboratories. Operations are conducted by COO, IPAC, and UW. This research used resources of the National Energy Research Scientific










Computing Center, a DOE Office of Science User Facility supported by the Office of Science of the U.S. Department of Energy under Contract No. DE-AC02-05CH11231. The 0.7 m GROWTH-India Telescope (GIT) is set up by the Indian Institute of Astrophysics (IIA) and the Indian Institute of Technology Bombay (IITB) with support from the Indo-US Science and Technology Forum (IUSSTF) and the Science and Engineering Research Board (SERB) of the Department of Science and Technology (DST), Government of India grant No. IUSSTF/PIRE Program/GROWTH/2015-16. It is located at the Indian Astronomical Observatory, IIA at Hanle, Ladakh (India). This publication has made use of data collected at Lulin Observatory, partly supported by MoST grant 105-2112-M-008-024-MY3. The KPED team thanks the National Science Foundation and the National Optical Astronomical Observatory for making the Kitt Peak 2.1 m telescope available. We thank the observatory staff at Kitt Peak for their efforts to assist Robo-AO KP operations. The KPED team thanks the National Science Foundation, the National Optical Astronomical Observatory, the Caltech Space Innovation Council, and the Murty family for support in the building and operation of KPED. SED Machine is based upon work supported by the National Science Foundation under grant No. 1106171. The Palomar Gattini-IR project thanks the Mount Cuba Foundation, Heising-Simons Foundation, the ANU Futures Scheme, the Binational Science Foundation, and Caltech for generous support.

G.C.A. and V.B. acknowledge partial support from SERB and IUSSTF. J.S. acknowledges support from the Knut and Alice Wallenberg Foundation. E.O. is grateful for support by a grant from the Israeli Ministry of Science, ISF, Minerva, BSF, BSF transformative program, and the I-CORE Program of the Planning and Budgeting Committee and The Israel Science Foundation (grant No. 1829/12). P.G. is supported by NASA Earth and Space Science Fellowship (ASTRO18F-0085). C.-C.N., A.P., and P.-C.Y. thank the funding from Ministry of Science and Technology (Taiwan) under grants 104-2923-M-008-004-MY5, 106-2112-M-008-007, 107-2119-M-008-012, 107-2119-M-008-014-MY2. E.B. and V.Z.G. acknowledge support from the University of Washington College of Arts and Sciences, Department of Astronomy, and the DIRAC Institute. University of Washington’s DIRAC Institute is supported through generous gifts from the Charles and Lisa Simonyi Fund for Arts and Sciences, and the Washington Research Foundation. E.B. acknowledges support from the Large Synoptic Survey Telescope, which is supported in part by the National Science Foundation through Cooperative Agreement 1258333 managed by the Association of Universities for Research in Astronomy (AURA), and the Department of Energy under Contract No. DE-AC02-76SF00515 with the SLAC National Accelerator Laboratory. Additional LSST funding comes from private donations, grants to universities, and in-kind support from LSSTC Institutional Members. E.B. is supported in part by the NSF AAG grant 1812779 and grant #2018-0908 from the Heising-Simons Foundation. M.W.C. is supported by the David and Ellen Lee Postdoctoral Fellowship at the California Institute of Technology. Part of this research was carried out at the Jet Propulsion Laboratory, California Institute of Technology, under a contract with the National Aeronautics and Space Administration. D.L.K. was supported by NSF grant AST-1816492. A.K.H.K. acknowledges support from the Ministry of Science and Technology of the Republic of

China (Taiwan) under grants 106-2628-M-007-005 and 107-2628-M-007-003. J.S.B. and J.M.-P. are partially supported by a Gordon and Betty Moore Foundation Data-Driven Discovery grant. H.K. thanks the LSSTC Data Science Fellowship Program, which is funded by LSSTC, NSF Cybertraining Grant #1829740, the Brinson Foundation, and the Moore Foundation; his participation in the program has benefited this work. S.A. acknowledges support from the PMA Division Medberry Fellowship at the California Institute of Technology. R.B., A.G., and J.S. acknowledge support from the G.R.E.A.T research environment funded by the Swedish National Science Foundation. J.S. acknowledges support by an Australian Government Research Training Program (RTP) Scholarship. M.R. acknowledges support from the European Research Council (ERC) under the European Union's Horizon 2020 research and innovation programme (grant agreement No. 759194 - USNAC).

### ORCID iDs

Michael W. Coughlin  <https://orcid.org/0000-0002-8262-2924>  
 Tomás Ahumada  <https://orcid.org/0000-0002-2184-6430>  
 Matthew J. Hankins  <https://orcid.org/0000-0001-9315-8437>  
 Mansi M. Kasliwal  <https://orcid.org/0000-0002-5619-4938>  
 Leo P. Singer  <https://orcid.org/0000-0001-9898-5597>  
 Eric C. Bellm  <https://orcid.org/0000-0001-8018-5348>  
 Igor Andreoni  <https://orcid.org/0000-0002-8977-1498>  
 S. Bradley Cenko  <https://orcid.org/0000-0003-1673-970X>  
 Jeff Cooke  <https://orcid.org/0000-0001-5703-2108>  
 Christopher M. Copperwheat  <https://orcid.org/0000-0001-7983-8698>  
 Jacob E. Jencson  <https://orcid.org/0000-0001-5754-4007>  
 Daniel A. Perley  <https://orcid.org/0000-0001-8472-1996>  
 Po-Chieh Yu  <https://orcid.org/0000-0001-8894-0854>  
 Varun Bhalerao  <https://orcid.org/0000-0002-6112-7609>  
 Michael C. B. Ashley  <https://orcid.org/0000-0003-1412-2028>  
 Rahul Biswas  <https://orcid.org/0000-0002-5741-7195>  
 David O. Cook  <https://orcid.org/0000-0002-6877-7655>  
 Virginia Cunningham  <https://orcid.org/0000-0003-2292-0441>  
 Antonino D'Ai  <https://orcid.org/0000-0002-5042-1036>  
 Dmitry A. Duv  <https://orcid.org/0000-0001-5060-8733>  
 Sara Frederick  <https://orcid.org/0000-0001-9676-730X>  
 Pradip Gatkine  <https://orcid.org/0000-0002-1955-2230>  
 Shaon Ghosh  <https://orcid.org/0000-0001-9901-6253>  
 Daniel A. Goldstein  <https://orcid.org/0000-0003-3461-8661>  
 V. Zach Golkhou  <https://orcid.org/0000-0001-8205-2506>  
 Ariel Goobar  <https://orcid.org/0000-0002-4163-4996>  
 Matthew J. Graham  <https://orcid.org/0000-0002-3168-0139>  
 Hidekazu Hanayama  <https://orcid.org/0000-0001-8221-6048>  
 Saurabh W. Jha  <https://orcid.org/0000-0001-8738-6011>  
 Albert K. H. Kong  <https://orcid.org/0000-0002-5105-344X>  
 David L. Kaplan  <https://orcid.org/0000-0001-6295-2881>  
 Shrinivas R. Kulkarni  <https://orcid.org/0000-0001-5390-8563>  
 Thomas Kupfer  <https://orcid.org/0000-0002-6540-1484>  
 Frank J. Masci  <https://orcid.org/0000-0002-8532-9395>  
 Paolo Mazzali  <https://orcid.org/0000-0001-6876-8284>  
 James D. Neill  <https://orcid.org/0000-0002-0466-1119>  
 Chow-Choong Ngeow  <https://orcid.org/0000-0001-8771-7554>

M. Pavana  <https://orcid.org/0000-0002-0000-1543>  
 Eran O. Ofek  <https://orcid.org/0000-0002-6786-8774>  
 Reed Riddle  <https://orcid.org/0000-0002-0387-370X>  
 Mickael Rigault  <https://orcid.org/0000-0002-8121-2560>  
 David L. Shupe  <https://orcid.org/0000-0003-4401-0430>  
 Jesper Sollerman  <https://orcid.org/0000-0003-1546-6615>  
 Eleonora Troja  <https://orcid.org/0000-0002-1869-7817>  
 Gaurav Waratkar  <https://orcid.org/0000-0003-3630-9440>  
 Yoichi Yatsu  <https://orcid.org/0000-0003-1890-3913>

### References

- Aasi, J., Abbott, B. P., Abbott, R., et al. 2015, *CQGra*, 32, 074001  
 Abbott, B. P., Abbott, R., Abbott, T. D., et al. 2017a, *PhRvL*, 119, 161101  
 Abbott, B. P., Abbott, R., Abbott, T. D., et al. 2017b, *ApJL*, 848, L13  
 Abbott, B. P., Abbott, R., Abbott, T. D., et al. 2017c, *ApJL*, 850, L39  
 Abbott, B. P., Abbott, R., Abbott, T. D., et al. 2017d, *Natur*, 551, 85  
 Abbott, B. P., Abbott, R., Abbott, T. D., et al. 2018, *LRR*, 21, 3  
 Abbott, B. P., Abbott, R., Abbott, T. D., et al. 2019, *PhRvX*, 9, 031040  
 Acernese, F., Agathos, M., Agatsuma, K., et al. 2015, *CQGra*, 32, 024001  
 Aghanim, N., Akrami, Y., Ashdown, M., et al. 2018, arXiv:1807.06209  
 Ahumada, T., Coughlin, M. W., Cenko, S. B., et al. 2018, GCN, 23515, 1  
 Ahumada, T., Coughlin, M. W., Staats, K., et al. 2019b, GCN, 24320, 1  
 Ahumada, T., Coughlin, M. W., Staats, K., et al. 2019c, GCN, 24343, 1  
 Ahumada, T., Coughlin, M. W., Staats, K., & Dekany, R. G. 2019a, GCN, 24198, 1  
 Alexander, K. D., Berger, E., Fong, W., et al. 2017, *ApJL*, 848, L21  
 Anand, S., Kasliwal, M., Coughlin, M. W., et al. 2019, GCN, 24311, 1  
 Andreoni, I., Anand, S., & Kasliwal, M. 2019a, GCN, 24349, 1  
 Andreoni, I., & Bellm, E. 2019, GCN, 24356, 1  
 Andreoni, I., Cenko, S. B., Masci, F., & Graham, M. 2019b, GCN, 24302, 1  
 Arcavi, I., Hosseinzadeh, G., Howell, D. A., et al. 2017b, *Natur*, 551, 64  
 Arcavi, I., Howell, D. A., McCully, C., et al. 2019, GCN, 24307, 1  
 Arcavi, I., McCully, C., Hosseinzadeh, G., et al. 2017a, *ApJL*, 848, L33  
 Ascenzi, S., Coughlin, M. W., Dietrich, T., et al. 2019, *MNRAS*, 486, 672  
 Bauswein, A., Baumgarte, T. W., & Janka, H.-T. 2013, *PhRvL*, 111, 131101  
 Bauswein, A., Just, O., Janka, H.-T., & Stergioulas, N. 2017, *ApJL*, 850, L34  
 Bellm, E. C., Kulkarni, S. R., Graham, M. J., et al. 2018, *PASP*, 131, 018002  
 Bhalerao, V., Kumar, H., Karambelkar, V., et al. 2019, GCN, 24201, 1  
 Blagorodnova, N., Neill, J. D., Walters, R., et al. 2018, *PASP*, 130, 035003  
 Bloom, J. S., Zucker, C., Schlafly, E., et al. 2019, GCN, 24337, 1  
 Breeveld, A. A., Kuin, N. P. M., Marshall, F. E., et al. 2019, GCN, 24296, 1  
 Buckley, D., Jha, S. W., Cooke, J., & Mogotsi, M. 2019, GCN, 24205, 1  
 Burke, J., Hiramatsu, D., Arcavi, I., et al. 2019, GCN, 24206, 1  
 Carini, R., Izzo, L., Palazzi, E., et al. 2019, GCN, 24252, 1  
 Castro-Tirado, A. J., Hu, Y. D., Li, X. Y., et al. 2019, GCN, 24214, 1  
 Cenko, B. S., Coughlin, M. W., Ghosh, S., et al. 2018, GCN, 22969, 1  
 Chambers, K. C., Magnier, E. A., Metcalfe, N., et al. 2016, arXiv:1612.05560  
 Chang, S. W., Wolf, C., Onken, C. A., et al. 2019a, GCN, 24260, 1  
 Chang, S.-W., Wolf, C., Onken, C. A., Luvaul, L., & Scott, S. 2019b, GCN, 24325, 1  
 Chornock, R., Berger, E., Kasen, D., et al. 2017, *ApJL*, 848, L19  
 Cook, D. O., Kasliwal, M. M., Van Sistine, A., et al. 2019, *ApJ*, 880, 7  
 Coughlin, M. W., Ahumada, T., Cenko, S. B., et al. 2019a, *PASP*, 131, 048001  
 Coughlin, M. W., Ahumada, T., Cenko, S. B., et al. 2018d, GCN, 23379, 1  
 Coughlin, M. W., Anand, S., & Ahumada, T. 2019b, GCN, 24223, 1  
 Coughlin, M. W., Antier, S., Corre, D., et al. 2019c, *MNRAS*, 489, 5775  
 Coughlin, M. W., Cenko, S. B., Ahumada, T., et al. 2018c, GCN, 23324, 1  
 Coughlin, M. W., Dekany, R. G., Duv, D. A., et al. 2019d, *MNRAS*, 485, 1412  
 Coughlin, M. W., Dietrich, T., Heinzel, J., et al. 2019e, arXiv:1908.00889  
 Coughlin, M. W., Dietrich, T., Margalit, B., & Metzger, B. D. 2019f, *MNRAS*, 489, L91  
 Coughlin, M. W., Singer, L. P., Ahumada, T., et al. 2018b, GCN, 22871, 1  
 Coughlin, M. W., Singer, L. P., Cenko, S. B., et al. 2018e, GCN, 22739, 1  
 Coughlin, M. W., Tao, D., Chan, M. L., et al. 2018a, *MNRAS*, 478, 692  
 Coulter, D. A., Foley, R. J., Kilpatrick, C. D., et al. 2017, *Sci*, 358, 1556  
 Cowperthwaite, P. S., Berger, E., Villar, V. A., et al. 2017, *ApJL*, 848, L17  
 Crawford, S. M., Still, M., Schellart, P., et al. 2010, *Proc. SPIE*, 7737, 25  
 De, K., Hankins, M., Adams, S. M., et al. 2019, GCN, 24306, 1  
 Dekany, R., Smith, R. M., Riddle, R., et al. 2019, *PASP*, submitted  
 Dichiaro, S., Gatkine, P., Durbak, J., et al. 2019, GCN, 24220, 1  
 Dimitriadis, G., Jones, D. O., Siebert, M. R., et al. 2019, GCN, 24358, 1

- Drout, M. R., Piro, A. L., Shappee, B. J., et al. 2017, *Sci*, **358**, 1570
- Duev, D. A., Mahabal, A., Masci, F. J., et al. 2019, *MNRAS*, **489**, 3582
- Evans, P. A., Cenko, S. B., Kennea, J. A., et al. 2017, *Sci*, **358**, 1565
- Finn, L. S., & Chernoff, D. F. 1993, *PhRvD*, **47**, 2198
- Flaugher, B., Diehl, H. T., Honscheid, K., et al. 2015, *AJ*, **150**, 150
- Flewelling, H. 2018, AAS Meeting, **231**, 436.01
- Goldstein, A., Veres, P., Burns, E., et al. 2017, *ApJL*, **848**, L14
- Golkhou, V. Z., Butler, N. R., Strausbaugh, R., et al. 2018, *ApJ*, **857**, 81
- Graham, M. J., Kulkarni, S. R., Bellm, E. C., et al. 2019, *PASP*, **131**, 078001
- Haggard, D., Nynka, M., Ruan, J. J., et al. 2017, *ApJL*, **848**, L25
- Hallinan, G., Corsi, A., Mooley, K. P., et al. 2017, *Sci*, **358**, 1579
- Hiramatsu, D., Arcavi, I., Burke, J., et al. 2019, GCN, 24194, 1
- Hosseinzadeh, G., Cowperthwaite, P. S., Gomez, S., et al. 2019, *ApJL*, **880**, L4
- Hotokezaka, K., Nakar, E., Gottlieb, O., et al. 2018, arXiv:1806.10596
- Hu, Y. D., Castro-Tirado, A. J., Li, X. Y., et al. 2019, GCN, 24324, 1
- Im, M., Kim, J., Paek, G. S. H., et al. 2019, GCN, 24318, 1
- Izzo, L., Carini, R., Benetti, S., et al. 2019, GCN, 24208, 1
- Jenson, J., De, K., Anand, S., et al. 2019, GCN, 24233, 1
- Jonker, P., Mata-Sanchez, D., Fraser, M., et al. 2019, GCN, 24221, 1
- Just, O., Bauswein, A., Pulpillo, R. A., Goriely, S., & Janka, H.-T. 2015, *MNRAS*, **448**, 541
- Kaiser, N., Burgett, W., Chambers, K., et al. 2010, *Proc. SPIE*, **7733**, 77330E
- Kann, D. A., Thoene, C., Stachie, C., et al. 2019, GCN, 24459, 1
- Kasliwal, M. M., Cannella, C., Bagdasaryan, A., et al. 2019b, *PASP*, **131**, 038003
- Kasliwal, M. M., Coughlin, M. W., Bellm, E. C., et al. 2019c, GCN, 24191, 1
- Kasliwal, M. M., Kasen, D., Lau, R. M., et al. 2019a, *MNRAS*, in press
- Kasen, D., Metzger, B., Barnes, J., Quataert, E., & Ramirez-Ruiz, E. 2017, *Natur*, **551**, 80
- Kasliwal, M. M., Nakar, E., Singer, L. P., et al. 2017, *Sci*, **358**, 1559
- Kasliwal, M. M., & Nissanke, S. 2014, *ApJL*, **789**, L5
- Kilpatrick, C. D., Foley, R. J., Kasen, D., et al. 2017, *Sci*, **358**, 1583
- Kong, A., Tan, H.-J., Yu, P.-C., Ngeow, C.-C., & Ip, W.-H. 2019, GCN, 24301, 1
- Kostrzewa-Rutkowska, Z., Hodgkin, S., Delgado, A., et al. 2019, GCN, 24354, 1
- Lattimer, J. M., & Schramm, D. N. 1974, *ApJL*, **192**, L145
- Li, L.-X., & Paczynski, B. 1998, *ApJL*, **507**, L59
- Li, W., Leaman, J., Chornock, R., et al. 2011, *MNRAS*, **412**, 1441
- LIGO Scientific Collaboration & Virgo Collaboration 2019a, GCN, 24141, 1
- LIGO Scientific Collaboration & Virgo Collaboration 2019b, GCN, 24237, 1
- LIGO Scientific Collaboration & Virgo Collaboration 2019c, GCN, 24377, 1
- LIGO Scientific Collaboration & Virgo Collaboration 2019d, GCN, 24098, 1
- LIGO Scientific Collaboration & Virgo Collaboration 2019e, GCN, 24069, 1
- LIGO Scientific Collaboration & Virgo Collaboration 2019f, GCN, 24168, 1
- LIGO Scientific Collaboration & Virgo Collaboration 2019g, GCN, 24228, 1
- LIGO Scientific Collaboration & Virgo Collaboration 2019h, GCN, 24228, 1
- Lipunov, V., Gorbvskoy, E., Tyurina, N., et al. 2019a, GCN, 24241, 1
- Lipunov, V., Tyurina, N., Gorbvskoy, E., et al. 2019b, GCN, 24326, 1
- Lipunov, V. M., Gorbvskoy, E., Kornilov, V. G., et al. 2017, *ApJL*, **850**, L1
- Mahabal, A., Rebbapragada, U., Walters, R., et al. 2019, *PASP*, **131**, 038002
- Margutti, R., Berger, E., Fong, W., et al. 2017, *ApJL*, **848**, L20
- Masci, F. J., Laher, R. R., Rusholme, B., et al. 2018, *PASP*, **131**, 018003
- McBrien, O., Smartt, S., Smith, K. W., et al. 2019, GCN, 24197, 1
- McCully, C., Hiramatsu, D., Howell, D. A., et al. 2017, *ApJL*, **848**, L32
- McCully, C., Hiramatsu, D., Howell, D. A., et al. 2019, GCN, 24295, 1
- Mészáros, P., & Rees, M. J. 1998, *ApJL*, **502**, L105
- Metzger, B. D. 2017, *LRR*, **20**, 3
- Metzger, B. D., Martínez-Pinedo, G., Darbha, S., et al. 2010, *MNRAS*, **406**, 2650
- Moore, A. M., & Kasliwal, M. M. 2019, *NatAs*, **3**, 109
- Morihana, K., Jian, M., & Nagayama, T. 2019a, GCN, 24219, 1
- Morihana, K., Jian, M., & Nagayama, T. 2019b, GCN, 24328, 1
- Morokuma, T., Ohta, K., Yoshida, M., et al. 2019, GCN, 24230, 1
- Muthukrishna, D., Narayan, G., Mandel, K. S., Biswas, R., & Hložek, R. 2019, *PASP*, **131**, 118002
- Nicholl, M., Berger, E., Kasen, D., et al. 2017, *ApJL*, **848**, L18
- Nicholl, M., Cartier, R., Pelisoli, I., et al. 2019, GCN, 24321, 1
- Nissanke, S., Kasliwal, M., & Georgieva, A. 2013, *ApJ*, **767**, 124
- Nordin, J., Brinnel, V., van Santen, J., et al. 2019, arXiv:1904.05922
- O'Brien, P. 2018, in 42nd COSPAR Scientific Assembly, Abstract E1.15-18-18
- Oke, J. B., & Gunn, J. E. 1982, *PASP*, **94**, 586
- Palmease, A., Soares-Santos, M., Santana-Silva, L., et al. 2019, GCN, 24312, 1
- Pavana, M., Kiran, B., Anupama, G., & Bhalerao, V. 2019, GCN, 24200, 1
- Perley, D. A., & Copperwheat, C. M. 2019, GCN, 24202, 1
- Perley, D. A., Copperwheat, C. M., & Taggart, K. L. 2019a, GCN, 24204, 1
- Perley, D. A., Copperwheat, C. M., & Taggart, K. L. 2019b, GCN, 24314, 1
- Perley, D. A., Copperwheat, C. M., & Taggart, K. L. 2019c, GCN, 24314, 1
- Pian, E., D'Avanzo, P., Benetti, S., et al. 2017, *Natur*, **551**, 67
- Piascik, A., Steele, I. A., Bates, S. D., et al. 2014, *Proc. SPIE*, **9147**, 91478H
- Radice, D., Perego, A., Zappa, F., & Bernuzzi, S. 2018, *ApJL*, **852**, L29
- Rhodes, L., Fender, R., Williams, D., et al. 2019, GCN, 24226, 1
- Richardson, D., III, R. L. J., Wright, J., & Maddox, L. 2014, *AJ*, **147**, 118
- Rigault, M., Neill, J. D., Blagorodnova, N., et al. 2019, *A&A*, **627**, A115
- Roberts, L. F., Kasen, D., Lee, W. H., & Ramirez-Ruiz, E. 2011, *ApJL*, **736**, L21
- Roberts, L. F., Lippuner, J., Duez, M. D., et al. 2017, *MNRAS*, **464**, 3907
- Rosswog, S. 2015, *IJMPD*, **24**, 1530012
- Rosswog, S., Feindt, U., Korobkin, O., et al. 2017, *CQGra*, **34**, 104001
- Savchenko, V., Ferrigno, C., Kuulkers, E., et al. 2017, *ApJL*, **848**, L15
- Schady, P., Chen, T. W., Schweyer, T., Malesani, D. B., & Bolmer, J. 2019, GCN, 24229, 1
- Shappee, B. J., Kochanek, C. S., Stanek, K. Z., et al. 2019, GCN, 24313, 1
- Shappee, B. J., Prieto, J. L., Grupe, D., et al. 2014, *ApJ*, **788**, 48
- Shappee, B. J., Simon, J. D., Drout, M. R., et al. 2017, *Sci*, **358**, 1574
- Singer, L. P., Cenko, S. B., Kasliwal, M. M., et al. 2013, *ApJL*, **776**, L34
- Singer, L. P., Kasliwal, M. M., Cenko, S. B., et al. 2015, *ApJ*, **806**, 52
- Smartt, S. J., Chen, T.-W., Jerkstrand, A., et al. 2017, *Natur*, **551**, 75
- Smith, K. W., Young, D. R., McBrien, O., et al. 2019, GCN, 24210, 1
- Smith, M. P., Nordisiek, K. H., Burgh, E. B., et al. 2006, *Proc. SPIE*, **6269**, 62692A
- Steele, I. A., Smith, R. J., Rees, P. C., et al. 2004, *Proc. SPIE*, **5489**, 679
- Tachibana, Y., & Miller, A. A. 2018, *PASP*, **130**, 128001
- Tan, H.-J., Yu, P.-C., Kong, A., et al. 2019a, GCN, 24274, 1
- Tan, H.-J., Yu, P.-C., Ngeow, C.-C., & Ip, W.-H. 2019b, GCN, 24193, 1
- Tanvir, N. R., Gonzalez-Fernandez, C., Levan, A. J., Malesani, D. B., & Evans, P. A. 2019, GCN, 24334, 1
- Tonry, J. L., Denneau, L., Heinze, A. N., et al. 2018, *PASP*, **130**, 064505
- Troja, E., Piro, L., van Eerten, H., et al. 2017, *Natur*, **551**, 71
- Troja, E., Watson, A. M., Becerra, R. L., et al. 2019, GCN, 24335, 1
- Utsumi, Y., Tanaka, M., Tominaga, N., et al. 2017, *PASJ*, **69**, 101
- Valenti, S., Sand, D. J., Yang, S., et al. 2017, *ApJL*, **848**, L24
- Waratkar, G., Kumar, H., Bhalerao, V., Stanzin, J., & Anupama, G. C. 2019, GCN, 24304, 1
- West, A. A., Morgan, D. P., Bochanski, J. J., et al. 2011, *AJ*, **141**, 97
- Wiersema, K., Levan, A. J., Fraser, M., et al. 2019, GCN, 24209, 1
- Wijers, R. A. M. J., Rees, M. J., & Mészáros, P. 1997, *MNRAS*, **288**, L51
- Wright, E. L., Eisenhardt, P. R. M., Mainzer, A. K., et al. 2010, *AJ*, **140**, 1868
- Wu, M.-R., Fernández, R., Martínez-Pinedo, G., & Metzger, B. D. 2016, *MNRAS*, **463**, 2323